04,10

Memristive properties of $Cu/(Co_{40}Fe_{40}B_{20})_x(SiO_2)_{100-x}/ZrO_2(Y)/Cr/Cu/Cr$ capacitor structures

© I.V. Babkina[1], A.V. Sitnikov[1,2], Yu.E. Kalinin[1], A.E. Nikonov[1], A.V. Ampilogov[1], A.R. Shakurov[1,¶], V.V. Rylkov[2]

[1] Voronezh State Technical University,
Voronezh, Russia
[2] National Research Center „Kurchatov Institute“,
Moscow, Russia
[¶] E-mail: Aleks.shakurov@mail.ru

Received April 3, 2025
Revised April 30, 2025
Accepted May 1, 2025

The article presents the results of studying the memristive properties of nanocomposite (NC) structures $Cu/NC/ZrO_2(Y)/Cr/Cu/Cr$/sitall based on NC $(Co_{40}Fe_{40}B_{20})_x(SiO_2)_{100-x}$. It is shown that the use of a dielectric layer of $ZrO_2(Y)$ and NC allows achieving practically significant memristive characteristics: resistive switching voltage (RSV) up to 2.5 V, resistance ratio $R_{\text{off}}/R_{\text{on}}$ more than 10. In this case, a multilevel nature of RS is realized with the temporary stability of induced resistive states of at least 1 h. Memristive structures demonstrate an insignificant spread of RS voltages from cycle to cycle (about 5%). At the same time, there is no need for a sample forming process to achieve stable RS. The presented results demonstrate the possibility of creating new memristive structures with a multifilament switching mechanism using NC with a metal phase concentration below the percolation threshold as one of the electrodes.

Keywords: Resistive switching, memristors, nanocomposite, zirconium oxide.

DOI: 10.61011/PSS.2025.05.61489.69-25

1. Introduction

Recently one of the priority areas for microelectronics development is the creation of the elements of a nonvolatile multi-level memory, which may model synapses while building the neuromorphic computing systems aimed at solving the objectives of the artificial intelligence: recognition of images and natural language, decision making, generalization, forecasting etc. The transistor-controlled crossbar-arrays of memristor elements with a random access in 1T1R architecture are considered promising. Besides, the memristor metal-insulator-metal (MIM) structures are currently one of the best known systems, whose manufacturing technology may be easily integrated with the technology for manufacturing of state-of-the-art CMOS microchips that operate under voltage of < 3 V [1–8].

The RS processes of memristors based on MIM structures are mainly associated with formation (damage) of filamentous conducting channels (filaments) in the thin dielectric film formed by oxygen vacancies or cations of metals (such as Cu^+, Ag^+), electrically migrated from the active electrode [1,2,7–13]. Filament formation is to a great extent random in nature, which is one of the root causes of memristor degradation in cyclic RS [1,2]. Another disadvantage of memristive MIM structures is associated with the fact that their stable operation usually requires moulding, which consists in applying rather high voltage to the structure, leading to formation of filaments (channels).

The peculiarity of our approach is using metal/nanocomposite/insulator/metal (M/NC/I/M) structures to create memristors [14–16]. In this case the transition to the conducting state depends on the percolation chains specified by the spatial position and concentration of metal nanogranules in NC. Therefore, resistance to RS turns out to be high, and the RS nature is multi-filament, which enables formation of multiple states under RS [15]. It was found that if $(Co_{40}Fe_{40}B_{20})_x(LiNbO_3)_{100-x}$ is used as NC, it became possible to implement the bipolar RS with the ratio of high-resistance (R_{off}) to low-resistance (Ron) resistive state $R_{\text{off}}/R_{\text{on}} \sim 100$ with the number of resistant RS cycles (durability) $> 10^5$ at the retention time of resistive stages exceeding 10^4 sec [14–16]. Besides, the high degree of memristor plasticity (multi-level nature of RS) made it possible to emulate important properties of biological synapses [16–19].

In this paper, another NC — $(Co_{40}Fe_{40}B_{20})_x(SiO_2)_{100-x}$ was used to develop M/NC/I/M structures, which on the one hand has homogeneous nanogranular structure [20], and on the other hand rather high thermal stability of structural and electrical properties [21]. In particular, we have recently studied the memristor structures $Cu/(Co_{40}Fe_{40}B_{20})_x(SiO_2)_{100-x}/LiNbO_3/Cr/Cu/Cr$/sitall, for which it was shown that they have the bipolar RS with ratio $R_{\text{off}}/R_{\text{on}} \approx 60$ and stability of cyclic RS above 10^4. Besides, stable multi-level RS of structures are observed after their thermal treatment to annealing temperature 350 °C [22].

The change in the composite composition enabled us to substantially improve the thermal resistance of M/NC/I/M structures without degradation of the main memristive

characteristics. At the same time, however, the timing stability of induced resistive states of the structure turned out to be not high enough. Therefore, it was decided to change the composition of the dielectric layer, having chosen a ZrO_2 stabilized with Y instead. Previous research [23–25] of memristive elements based on ZrO_2(Y) demonstrated their quite acceptable memristive characteristics for neuromorphic applications.

Therefore, the primary objective of this paper is to study the effect of ZrO_2, oxide stabilized with Y, at memristive properties of M/$(Co_{40}Fe_{40}B_{20})_x(SiO_2)_{100-x}$/$ZrO_2$(Y)/M structure.

2. Specimens and study methods

M/NC/I/M capacitor structures were obtained by ion beam sputtering, based on NC $(Co_{40}Fe_{40}B_{20})_x(SiO_2)_{100-x}$ (these composites will be hereinafter referred to as $(CoFeB)_x(SiO_2)_{100-x}$ for brevity). To synthesize layers of ZrO_2(Y), a target $ZrO_2:Y_2O_3$ (88/12 mass.%), was used, which was purchased in „Girmet LLC". The bottom electrode was three-layer Cr/Cu/Cr films, and the top electrode — Cu films (Figure 1).

The experimental specimens were synthesized using shadow masks on an ion-beam sputtering installation in the three technological processes described in detail in [22]. The thicknesses of the obtained layers were as follows, nm: 1000/250/15/100/1000/100 in accordance with the structure diagram shown in Figure 1. The composite was deposited from the composite target including a plate of $Co_{40}Fe_{40}B_{20}$ alloy with size of $280 \times 80 \times 10\,mm^3$ and 13 unevenly placed quartz subsamples with size of $80 \times 10 \times 2\,mm^3$. Uneven arrangement of subsamples made it possible to produce NC films with different ratio of concentrations of dielectric and metallic phases x within the limits from 19 to 42 at.% in a single deposition cycle. The dielectric was deposited from a ceramic target ZrO_2:Y_2O_3 (88/12 mass.%).

The vacuum ion-beam sputtering installation comprises an oil-free pumping system, which allows to pull vacuum in the chamber of at least $1 \cdot 10^{-6}$ Torr. Gases with purity of 99.999 % min were used for deposition.

The elemental composition of NC was determined using Oxford INCA Energy 250 energy-dispersive X-ray attachment on JEOL JSM-6380 LV scanning electron microscope. The accuracy of identification of the composition of the specimens was $\delta x = \pm 1$ at.% and was determined by their size, discrete location on the substrates. The structural analysis was performed by X-ray method on diffractometer BRUKER D2 PHASER.

The current-voltage curve (CVC) of M/NK/D/M structures and their memristive properties were measured using a KEITHLEY 2450 multifunctional source-measuring device and an analytical probe station in current-limited mode. The CVC of the structures was measured with the bottom electrode grounded and the bias voltage U of the top electrode was scanned linearly in the sequence from

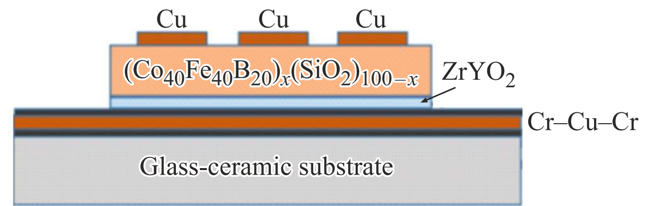

Figure 1. Sketch of experimental specimens M/NC/I/M.

$0 \to +U_{max} \to -U_{max} \to 0\,V$ in steps of 0.1 V. The rate of voltage change was 1 V/s.

3. Results and discussion

The structure of the produced layers $(CoFeB)_x(SiO_2)_{100-x}$ and ZrO_2(Y) was investigated by X-ray method on the films with thickness of around 1 μm, deposited on the surface of single-crystal Si (100).

X-ray diffraction from film ZrO_2(Y) (Figure 2) shows its crystalline structure. Mathematical processing of the obtained diffraction pattern was carried out by Pawley method in the environment of Topaz software. The best match with the experimental data was obtained when a triclinic crystalline lattice was used as a model lattice cell with the parameters given in the table on the insert to Figure 2 (see also the detailed results of the numerical modeling in paper [26]). Since the parameter of the cubic lattice ZrO_2 is 5.14 Å, the obtained crystalline structure ZrO_2(Y) may be characterized as pseudocubic with a minor change in the prameter of lattice ZrO_2 and angles of the cubic lattice cell of Zr oxide by introduction of Y atoms.

X-ray diffraction of NC $(CoFeB)_x(SiO_2)_{100-x}$ found no crystalline structure both in dielectric and metal phases in the entire studied range of concentrations (Figure 3). Besides, the observed features in the spectra of low-angle diffraction of X-ray radiation from NC films (insert to Figure 3) may be related to the presence of an ordered

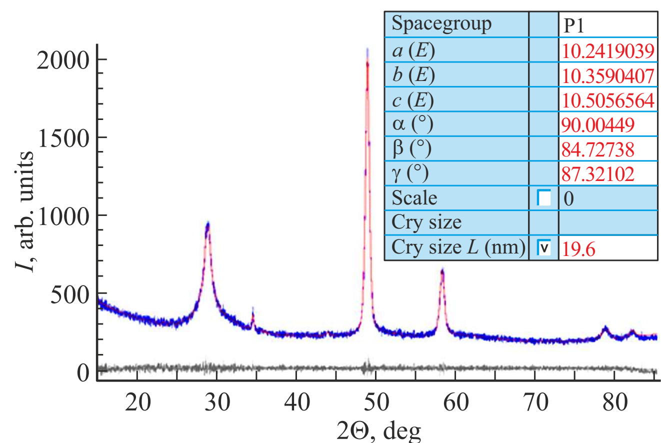

Figure 2. ZrO_2(Y) film diffraction pattern.

structure in the NC in the relative arrangement of the metal granules. By the position of the maximum you can assess the average distance between the centers of the granules (parameter d on insert to Figure 3), which is around 3 nm and increases with the increase of the metal phase concentration.

Figure 4 shows CVC curves of Cu/$(CoFeB)_x(SiO_2)_{100-x}$/ZrO_2(Y)/Cr/Cu/Cr/sitall structures, which in the entire studied range of NC metal phase concentrations demonstrate hysteresis. However, only starting from $x \geq 21.4$ at.%, in

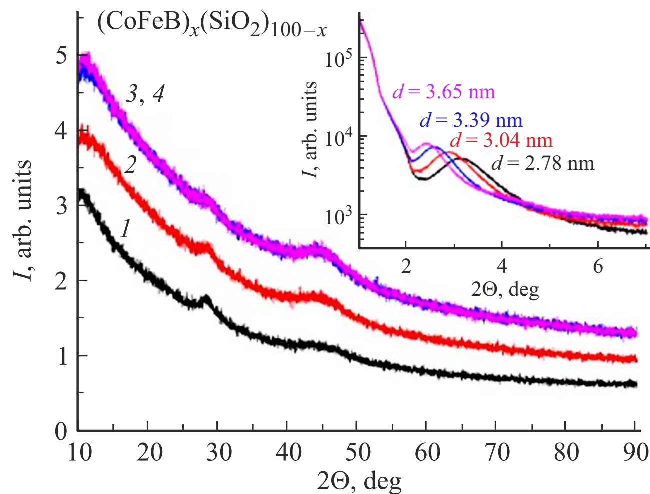

Figure 3. Diffraction patterns of NC $(CoFeB)_x(SiO_2)_{100-x}$ films with various concentration of metal phase: *1* — 14.1 at.%, *2* — 28.9 at.%, *3* — 38.9 at.%, *4* — 42.1 at.%. The insert presents diffraction patterns of films obtained by the low-angle scattering method.

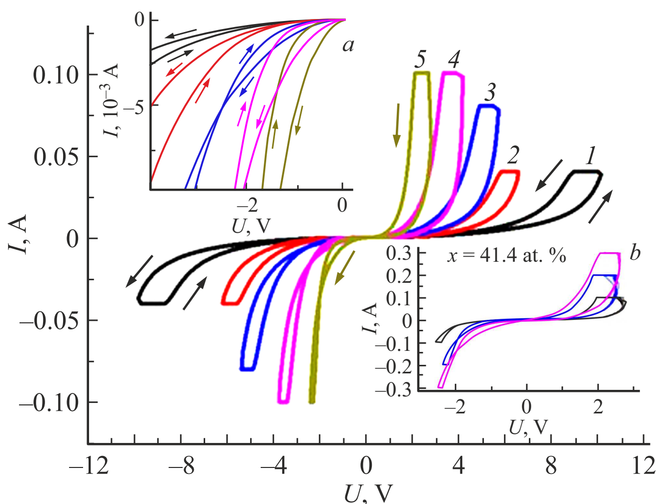

Figure 4. CVC of memristive element Cu/$(CoFeB)_x(SiO_2)_{100-x}$/ZrO_2(Y)/Cr/Cu/Cr/sitall with various concentration of metal phase: *1* — 14.1 at.%, *2* — 18.9 at.%, *3* — 21.4 at.%, *4* — 26.4 at.%, *5* — 41.4 at.%. On inserts: *a* — Negative branches of structures CVC in the region of low currents and voltages; *b* — CVC of the structure with metal phase concentration 41.4 at.% at various limitation currents.

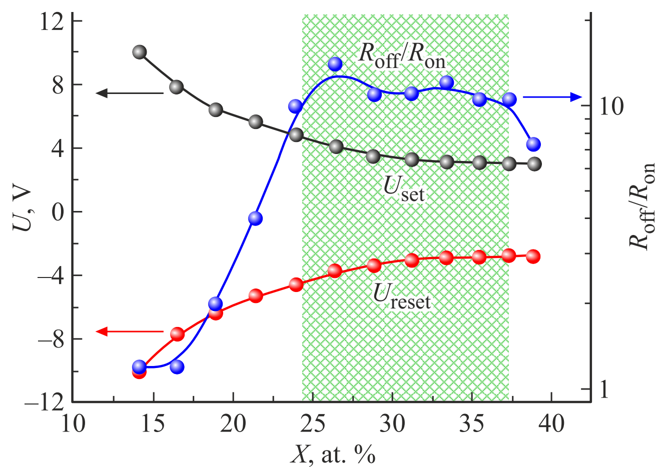

Figure 5. Concentration dependences of parameters R_{off}/R_{on}, U_{set} and U_{reset} for structure Cu/$(CoFeB)_x(SiO_2)_{100-x}$/ZrO_2(Y)/Cr/Cu/Cr/sitall.

the negative region of CVC, one may observe the effect of current drop at reverse scanning by voltage (towards positive values; see insert on Figure 4), which indicates manifestation of a bipolar RS. The voltages of switching from high-resistance to low-resistance state ($R_{off} \rightarrow R_{on}$) and from low-resistance to high-resistance state ($R_{on} \rightarrow R_{off}$) differ substantially depending on the metal phase concentration in NC. Besides, as value x increases, current through the specimen, where resistant RS are observed, increases.

More detailed analysis of concentration dependences of memristive properties for Cu/$(CoFeB)_x(SiO_2)_{100-x}$/ZrO_2(Y)/Cr/Cu/Cr/sitall structure is given in Figure 5.

4. Analysis of memristive properties of obtained structures

The obtained results are consistently explained within the framework of the ideas on the multi-filament RS in the layer of ZrO_2(Y) dielectric, the position of which is specified by conducting channels from granule chains in NC [15]. As the metal phase concentration increases in NC $(CoFeB)_x(SiO_2)_{100-x}$, the decrease in the resistance of channels (R_{ch}) and their density increase are observed. Decrease of R_{ch} causes redistribution of voltage in the channel–dielectric chain. Besides, the voltage increases on the layer ZrO_2(Y), which causes RS. Current through the specimen is specified by density of induced filaments, which is proportionate to the density of conducting channels in NC. However, in these structures the resistive heating of NC and dielectric plays a significant role. As it was shown in paper [27], if the given capacity exceeds 0.1 W/mm^2, the NC film is subjected to noticeable heating, and its resistance prior to the percolation threshold decreases. The resistance of the dielectric film may behave in a similar way. For this reason, a symmetrical hysteresis is observed in the CVC of structures

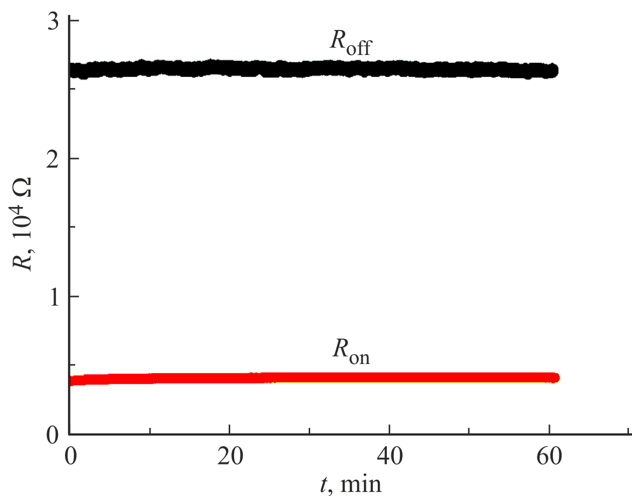

Figure 6. Timing dependence of resistance of induced resistive ON an OFF states for memristor structures $Cu/(CoFeB)_{35.5}(SiO_2)_{64.5}/ZrO_2(Y)/Cr/Cu/Cr$/sitall.

$Cu/(CoFeB)_x(SiO_2)_{100-x}/ZrO_2(Y)/Cr/Cu/Cr$/sitall with $x < 21.4$ at.%, related in essence to the heating of the structures in process of CVC measurement. At higher concentrations of NC metal phase you start observing the RS process. Besides, in process of transition $R_{off} \to R_{on}$ the heat exposure increases the CVC hysteresis, and on the contrary, in process of transition from R_{on} to R_{off} this effect decays, causing a decrease in the hysteresis loop in the region of negative voltages on the structure. Under such conditions, only at the low absolute values of negative voltage the specimen shows a process of structure transition to the high-resistance state (see insert *a* in Figure 4). You should also note the repeatability of the structure CVC parameters from a cycle to a cycle and absence of the process of memristive structures molding to bring them to the mode of reversible resistive switching, which manifests in the absence of the need for noticeable increase of voltages and operating currents to observe the first RS (see insert *b* in Figure 4).

The important property of memristors is preservation of induced resistive states for the period of time (retention time). Figure 6 shows dependences R_{off} and R_{on} on time for the structure $Cu/(CoFeB)_{35.5}(SiO_2)_{64.5}/ZrO_2(Y)/Cr/Cu/Cr$/sitall, which show that the high-resistance and low-resistance states are maintained well for at least an hour.

An unexpected property of the structures was high plasticity of resistive states, i.e. ability to switch to the state with actually any value of resistance in the range from R_{on} to R_{off}. Figure 7 demonstrates the opportunity to specify random values of resistance in this range, besides, the values are stable in the time interval of 300 s min. Besides, you can both decrease and increase the resistance values.

Both plasticity and timing stability of induced resistive states should manifest in quasistatic mode of CVC measurement. In this case after RS of the structure to a certain state with the fixed voltage, its current resistance is measured for some time. If you then calculate the relative value of resistance variation at the current voltage value, you may see qualitatively how the process of transition from state R_{on} to R_{off}, and the reverse process of transition from R_{off} to R_{on}, and the voltage range which has no impact at the change of the current value of induced resistance. The modes of conducted measurements: increment of voltage 0.1 V, time of resistance measurement at current voltage 10 sec, number of measurements 10. The obtained dependence is shown in Figure 8.

In the region of positive values, the degree of decrease in the values R is observed at voltages of around 2 V, and it increases as the displacement increases to the moment of complete switching at 2.5 V. In the region of transition from state R_{on} to R_{off} at negative voltages on the top electrode there is a region of voltages from -1 to -2.5 V, where the relatively smooth increase in specimen resistance is observed. The RS regions spread along the voltage scale describe qualitatively the structure plasticity (see Figure 7),

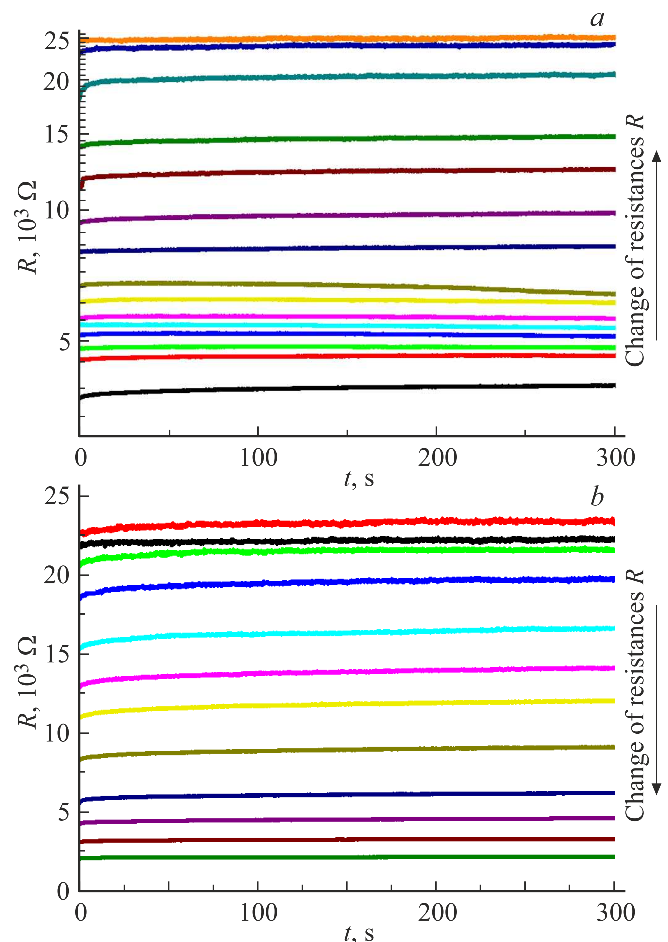

Figure 7. Timing dependence of resistance of induced resistive states for memristor structures $Cu/(CoFeB)_{35.5}(SiO_2)_{64.5}/ZrO_2(Y)/Cr/Cu/Cr$/ sitall. The arrows show the direction of the resistance change towards its increase (*a*) and decrease (*b*).

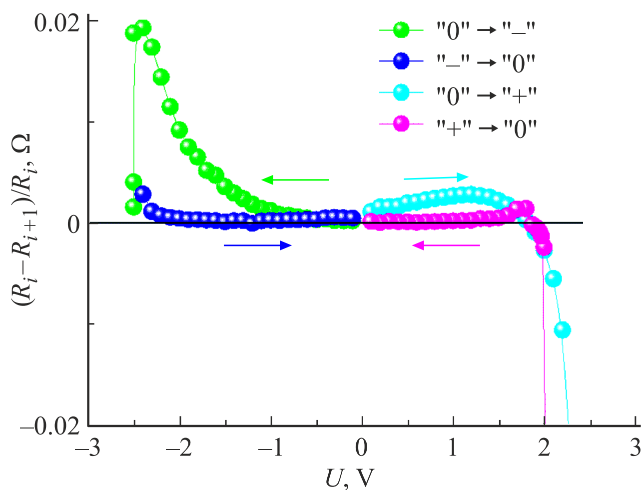

Figure 8. Relative speed of resistance change for structure $Cu/(CoFeB)_{35.5}(SiO_2)_{64.5}/ZrO_2(Y)/Cr/Cu/Cr$/sitall vs the applied voltage.

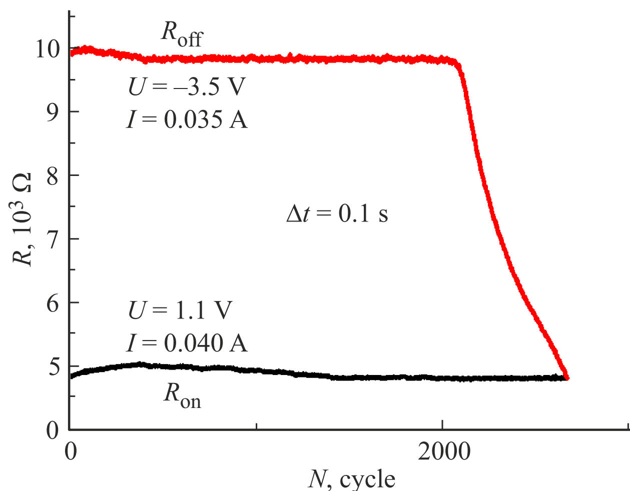

Figure 9. Switching of resistive states in memristor structures $Cu/(CoFeB)_{35.5}(SiO_2)_{64.5}/ZrO_2(Y)/Cr/Cu/Cr$/sitall.

and absence of significant changes of resistance in the voltage range from -1 V to 2 V characterize the timing stability of induced resistive states (Figure 6).

The important parameter of memristive structures is their ability of multiple cyclic RS between high-resistance and low-resistance resistive stages (durability). For the investigated structure $Cu/(CoFeB)_{35.5}(SiO_2)_{64.5}/ZrO_2(Y)/Cr/Cu/Cr$/sitall one may observe around 2000 reversible resistive switches (see Figure 9). At higher quantity of RS, the amplitude degradation is observed — R_{off} approaches R_{on} as the number of switches rises. The reason for such behavior requires further research. However, you may assume that the process of degradation is probably related to the interaction of the oxygen atoms that participate in the formation of oxygen vacancies, with boron atoms in NC and on NC interface with the top electrode. It should be noted that relatively small quantity of RS between the extreme states — this is a frequent phenomenon for very plastic memristors [28]. Besides, in process of a smooth stepwise RS between the extreme states of such nature the memristors may experience by orders more RS (see Annex in [28]). Such smooth RS are planned for the future as well.

5. Conclusion

Studies of memristive characteristics of the $Cu/(CoFeB)_x(SiO_2)_{100-x}/ZrO_2(Y)/Cr/Cu/Cr$/sitall structure have shown that in the NC metal phase concentration range from 21 at.% to 43 at.% the specimens demonstrate reversible bipolar resistive switches with minor variation of VCV curves from a cycle to a cycle. Besides, the developed memristors require no molding to achieve the stable reversible RS. The value of switching voltage from R_{off} to R_{on} states decreases as x increases and reaches ± 2.5 V at $x = 37-42$ at.% at the ratio of $R_{off}/R_{on} \sim 10$. It is shown that the obtained samples store the induced resistive states for at least one hour and have the multi-level nature of RS (at least 16 states). Besides, the number of cycles of the reversible RS in process of switching between the extreme states is around 2000.

The conducted research shows the possibility to create new multi-level memristive structures when metal-insulator nanocomposite is used as one of electrodes with metal phase concentration below the percolation threshold.

Funding

This study was financially supported by the Russian Science Foundation, project No. 25-29-00215.

Conflict of interest

The authors declare that they have no conflict of interest.

References

[1] D. Ielmini. Semicond. Sci. Technol. **31**, 063002 (2016).
[2] W. Banerjee, Q. Liu, H. Hwang. J. Appl. Phys., **127**, 051101 (2020).
[3] Y. Zhang, Z. Wang, J. Zhu, Y. Yang, M. Rao, W. Song, Y. Zhuo, X. Zhang, M. Cui, L. Shen, R. Huang, J. Yang. Appl. Phys. Rev., **7**, 011308 (2020).
[4] D. Ham, H. Park, S. Hwang, K. Kim. Nat. Electron., **4**, 635 (2021).
[5] Q. Xia, J.J. Yang. Nat. Mater., **18**, 309 (2019).
[6] M. Zhuk, S. Zarubin, I. Karateev, Y. Matveyev, E. Gornev, G. Krasnikov, D. Negrov, A. Zenkevich. Front. Neurosci., **14**, 94 (2020).
[7] A. Mikhaylov, A. Belov, D. Korolev, I. Antonov, V. Kotomina, A. Kotina, E. Gryaznov, A. Sharapov, M. Koryazhkina, R. Kryukov, S. Zubkov, A. Sushkov, D. Pavlov, S. Tikhov, O. Morozov, D. Tetelbaum. Adv. Mater. Technol., **5**, 1900607 (2020).

[8] Z. Wang, H. Wu, G.W. Burr, C.S. Hwang, K.L. Wang, Q. Xia, J.J. Yang. Nature Rev. Mater. **5**, 173 (2020).

[9] J. del Valle, J.G. Ramirez, M.J. Rozenberg, I.K. Shuller. J. Appl. Phys., **124**, 211101 (2018).

[10] Y. Li, Z. Wang, R. Midya, Q. Xia, J.J. Yang. J. Phys. D: Appl. Phys., **51**, 503002 (2018).

[11] D.-H. Kwon, K.M. Kim, J.H. Jang, J.M. Jeon, M.H. Lee, G.H. Kim, X.-S. Li, G.-S. Park, B. Lee, S. Han, M. Kim, C.S. Hwang. Nat. Nanotechnol., **5**, 153 (2010).

[12] J.-Y. Chen, C.-W. Huang, C.-H. Chiu, Y.-T. Huang, W.-W. Wu. Adv. Mater., **27**, 5028 (2015).

[13] H. Jiang, L. Han, P. Lin, Z. Wang, M.H. Jang, Q. Wu, M. Barnell, J.J. Yang, H.L. Xin, Q. Xia. Sci. Rep., **6**, 28525 (2016).

[14] V.V. Rylkov, S. Nikolaev, V.A. Demin, A.V. Emelyanov, A.V. Sitnikov, K.E. Nikiruy, V.A. Levanov, M.Yu. Presnyakov, A.N. Taldenkov, A.L. Vasiliev, K.Yu. Chernoglazov, A. Vedeneev, Yu.E. Kalinin, A.B. Granovsky, V. Tugushev, A.S. Bugaev. J. Exp. Theor. Phys., **126**, 367 (2018).

[15] M.N. Martyshov, A.V. Emelyanov, V.A. Demin, K.E. Nikiruy, A.A. Minnekhanov, S.N. Nikolaev, A.N. Taldenkov, A.V. Ovcharov, M.Yu. Presnyakov, A.V. Sitnikov, A.L. Vasiliev, P.A. Forsh, A.B. Granovskiy, P.K. Kashkarov, M.V. Kovalchuk, V.V. Rylkov. Phys. Rev. Applied **14**, 034016 (2020).

[16] K.E. Nikiruy, A.V. Emelyanov, V.A. Demin, A.V. Sitnikov, A.A. Minnekhanov, V.V. Rylkov, P.K. Kashakrov, M.V. Kovalchuk. AIP Advances, **9**, 065116 (2019).

[17] A.V. Emelyanov, K.E. Nikiruy, A.V. Serenko, A.V. Sitnikov, M.Yu. Presnyakov, R.B. Rybka, A.G. Sboev, V.V. Rylkov, P.K. Kashkarov, M.V. Kovalchuk. Nanotechnology, **31**, 045201 (2020).

[18] K.E. Nikiruy, I.A. Surazhevsky, V.A. Demin, A.V. Emelyanov. Phys. Status Solidi A, **217**, *18*, 1900938 (2020).

[19] I.A. Surazhevsky, V.A. Demin, A.I. Ilyasov, A.V. Emelyanov, K.E. Nikiruy, V.V. Rylkov, S.A. Shchanikov, I.A. Bordanov, S.A. Gerasimova, D.V. Guseinov, N.V. Malekhonova, D.A. Pavlov, A.I. Belov, A.N. Mikhaylov, V.B. Kazantsev, D. Valenti, B. Spagnolo, M.V. Kovalchuk. Chaos, Solitons and Fractals, **146**, 110890 (2021).

[20] A.V. Sitnikov. Materialovedenie, **3**, 49, (2010). (in Russian).

[21] S.A. Gridnev, Yu.E. Kalinin, A.V. Sitnikov, O.V. Stogney. Nelinejnye yavleniya v nano- i mikrogeterogennykh sistemakh, OOO „Izdatel'stvo„ BINOM. Laboratoriya Znanii". Moscow. (2012), P. 358. (in Russian).

[22] A.V. Sitnikov, Yu.E. Kalinin, I.V. Babkina, A.E. Nikonov, A.R. Shakurov, M.N. Kopytin. Fizika tverdogo tela, **66**, *10*, 1713 (2024). (in Russian).

[23] O.N. Gorshkov, I.N. Antonov, A.I. Belov, A.P. Kasatkin, A.N. Mikhaylov. Tech. Phys. Lett. **40**, 101 (2014).

[24] D.V. Guseinov, D.I. Tetelbaum, A.N. Mikhaylov, A.I. Belov, M.E. Shenina, D.S. Korolev, I.N. Antonov, A.P. Kasatkin, O.N. Gorshkov, E.V. Okulich, V.I. Okulich, A.I. Bobrov, N.V. Malekhonova, D.A. Pavlov, E.G. Gryaznov. Int. J. Nanotechnol. **14**, 604 (2017).

[25] A.N. Mikhaylov, M.N. Koryazhkina, D.S. Korolev, A.I. Belov, E.V. Okulich, V.I. Okulich, I.N. Antonov, R.A. Shuisky, D.V. Guseinov, K.V. Sidorenko, M.E. Shenina, E.G. Gryaznov, S.V. Tikhov, D.O. Filatov, D.A. Pavlov, D.I. Tetelbaum, O.N. Gorshkov, B. Spagnolo, A.V. Emelyanov, K.E. Nikiruy. Metal Oxides for Non-volatile Memory: Materials, Technology and Applications, Elsevier Inc., (2022), C. 109.

[26] M.A. Parkes, K. Refson, M. D'avezac, G.J. Offer, N.P. Brandon, N.M. Harrison. J. Phys. Chem. A, **119**, *24*, 6412 (2015).

[27] A.V. Sitnikov, Yu.E. Kalinin, I.V. Babkina, A.E. Nikonov, D.S. Pogrebnoy, A.R. Shakurov. Zhurnal tekhnicheskoy fiziki, **95**, *1*, 107 (2025). (in Russian).

[28] H. Yeon, P. Lin, C. Choi, S.H. Tan, Y. Park, D. Lee, J. Lee, F. Xu, B. Gao, H. Wu, H. Qian, Y. Nie, S. Kim, J. Kim. Nature Nanotechnology, **15**, 574 (2020)

Translated by M.Verenikina